Abdominal Radiology (2020) 45:2268–2273
https://doi.org/10.1007/s00261-020-02437-2

SPECIAL SECTION: DISTINGUISHED PAPERS FROM JSAR

Mass-forming hepatic cryptococcosis: a mimicker of metastatic tumors

Sodai Hoshiai[1,2] · Takashi Hiyama[2,3] · Hiroshi Kawasaki[4] · Hitoaki Saitoh[5] · Kensaku Mori[1] · Katsuhiro Nasu[1] · Taishi Amano[1] · Manabu Minami[1]

Published online: 8 February 2020

Abstract
This report provides the first imaging report of isolated intrahepatic cryptococcosis. An 83-year-old man was incidentally pointed out of hepatic nodules. CT revealed four well-defined nodules of 21 mm, 15 mm, 7 mm, and 5 mm in diameter without contrast enhancement. Two nodules displayed central hyperattenuation and the others were totally hyperattenuating. MRI showed that the nodules were hypointense relative to normal liver parenchyma on T1- and T2-weighted images. 18F-FDG PET imaging revealed no obvious increased uptake of nuclear species into the liver nodules. Partial resection of the three largest hepatic nodules was performed based on a preoperative diagnosis of hepatic metastasis from known sigmoid colon cancer. All three resected nodules were composed mainly of necrotic tissue with peripheral histiocytic aggregates and numerous yeast-like cells. The final diagnosis was hepatic cryptococcosis.

Keywords Cryptococcus · Cryptococcosis · Hepatic cryptococcosis · Liver cryptococcosis

Introduction

Cryptococcosis is a ubiquitous infectious disease caused by the pathogenic fungus *Cryptococcus*. It tends to mainly affect the lungs and central nervous system [1, 2], and imaging findings of pulmonary and central nervous system cryptococcosis have been previously reported [3–6]. Although some cases of hepatic cryptococcosis have been reported, most were due to disseminated cryptococcosis [7–10]. Isolated hepatic cryptococcosis presenting as intrahepatic nodules has not been reported. We present a case of human cryptococcosis of the liver with radiologic findings including computed tomography (CT), magnetic resonance imaging (MRI), and 18-fluorine fluorodeoxyglucose positron emission tomography (18F-FDG PET), and pathological confirmation.

Case

An 83-year-old man visited a local hospital with left shoulder pain, and computed tomography (CT) examination was performed following chest radiography. The non-contrast-enhanced CT revealed no abnormality besides the presence of four hepatic nodules. His left shoulder pain subsided spontaneously within a few weeks. He was referred to our hospital for diagnosis of the hepatic nodules.

The patient had a history of hormone therapy for prostate cancer three years ago but chose to terminate therapy two years ago. Upon examination, the aspartate aminotransferase (AST) level was 42 U/L (normal range 8–38 U/L); lactate dehydrogenase (LDH) and alkaline phosphatase (ALP) were 341 U/L (normal range 110–240 U/L) and 350 U/L (normal range 104–338 U/L), respectively; tumor markers of carbohydrate antigen 19–9 (CA 19–9), carcinoembryonic antigen (CEA), alpha-fetoprotein (AFP), and prostate-specific antigen (PSA) levels were normal. Laboratory test results are summarized in Table 1. Serology for viral hepatitis and

✉ Sodai Hoshiai
hoshiai@md.tsukuba.ac.jp

1 Department of Radiology, Faculty of Medicine, University of Tsukuba, 1-1-1 Tennodai, Tsukuba, Ibaraki 305-8575, Japan

2 Department of Radiology, Ibaraki Prefectural Central Hospital, Koibuchi 6528, Kasama, Ibaraki 309-1793, Japan

3 Department of Radiology, National Cancer Center Hospital East, 6-5-1 Kashiwanoha, Kashiwa, Chiba 227-8577, Japan

4 Department of Surgery, Ibaraki Prefectural Central Hospital, Koibuchi 6528, Kasama, Ibaraki 309-1793, Japan

5 Department of Pathology, Ibaraki Prefectural Central Hospital, Koibuchi 6528, Kasama, Ibaraki 309-1793, Japan

Table 1 Laboratory data

Variable	Reference range	At the initial visit
Hemoglobin (g/dL)	12.4–16.6	14.5
Platelet count (per μL)	127,000–348,000	141,000
White blood cell count (per μL)	4000–9000	4,100
Differential count (%)		
Neutrophils	47.2–75.2	42.1
Lymphocytes	20.5–51.1	47.7
Monocytes	2–10	5.1
Eosinophils	0–5.5	4.1
Basophils	0–1.5	1.0
Alanine aminotransferase (U/L)	4–44	39
Aspartate aminotransferase (U/L)	8–38	42
Alkaline phosphatase (U/L)	104–338	350
Lactate dehydrogenase (U/L)	110–240	341
γ-glutamyl transferase (U/L)	7–70	22
Total bilirubin (mg/dL)	0.3–1.2	1.0
Amylase (U/L)	37–125	84
Carbohydrate antigen 19–9 (U/mL)	0–37	< 2.0
Carcinoembryonic antigen (ng/mL)	0–5	2.7
α-fetoprotein (ng/mL)	0–10	7.2
Prostate-specific antigen (ng/mL)	0–4	1.104

human immunodeficiency virus was negative and there was no evidence of diabetes mellitus.

The largest hepatic nodule in segment 3 was a well-circumscribed round lesion of 21 mm in diameter. It was slightly hypoattenuating relative to normal liver parenchyma, with a central hyperattenuating area on non-contrast-enhanced CT (Fig. 1a). On contrast-enhanced CT with iomeprol (Iomeron 350, 350 mg I/mL; Eisai, Tokyo, Japan), enhancement of the nodule was not observed in arterial, portal, and delayed phases (Fig. 1b–d). The second-largest hepatic nodule of 15 mm in diameter in segment 7 presented similar radiological findings to the previously mentioned largest nodule in segment 3 (Fig. 2). The remaining two nodules were hyperattenuating and were identified in segments 3 and 4 as having diameters of 7 mm and 5 mm, respectively (Fig. 2a). MRI of the upper abdomen was performed before and after the administration of intravenous contrast material, gadolinium ethoxybenzyl diethylenetriamine pentaacetic acid (Gd-EOB-DTPA; Bayer Health Care, Berlin, Germany). T2-weighted image (repetition time (TR)/echo time (TE) = 800 ms/68 ms, slice thickness (ST) = 6 mm) showed that the largest nodule in segment 3 was slightly hypointense relative to normal liver parenchyma, with a peripheral ring-like hyperintense area (Fig. 3c). On the T1-weighted image (TR/TE = 206 ms/4.9 ms, ST = 6 mm), the nodule was hypointense relative to normal liver parenchyma with a peripheral hypo- and hyper-intense rim (Fig. 3a, b). Chemical shift image revealed that the nodule contained no lipid component (Fig. 3a, b). Diffusion-weighted image

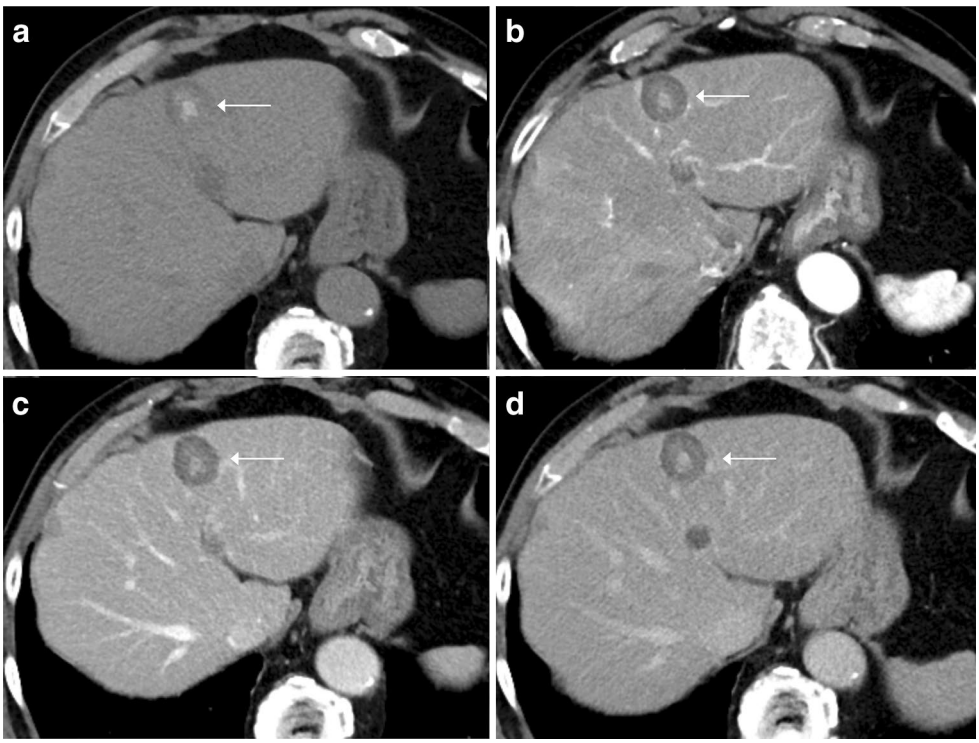

Fig. 1 Non-contrast and contrast-enhanced CT images. **a** The largest hepatic nodule (white arrow) in segment 3 was a well-circumscribed round lesion with a diameter of 21 mm and was slightly hypoattenuating relative to normal liver parenchyma, with central hyperattenuating areas on non-contrast-enhanced CT. **b–d** On contrast-enhanced CT, no enhancement of the nodule was observed in arterial (**b**), portal (**c**) and delayed (**d**) phases

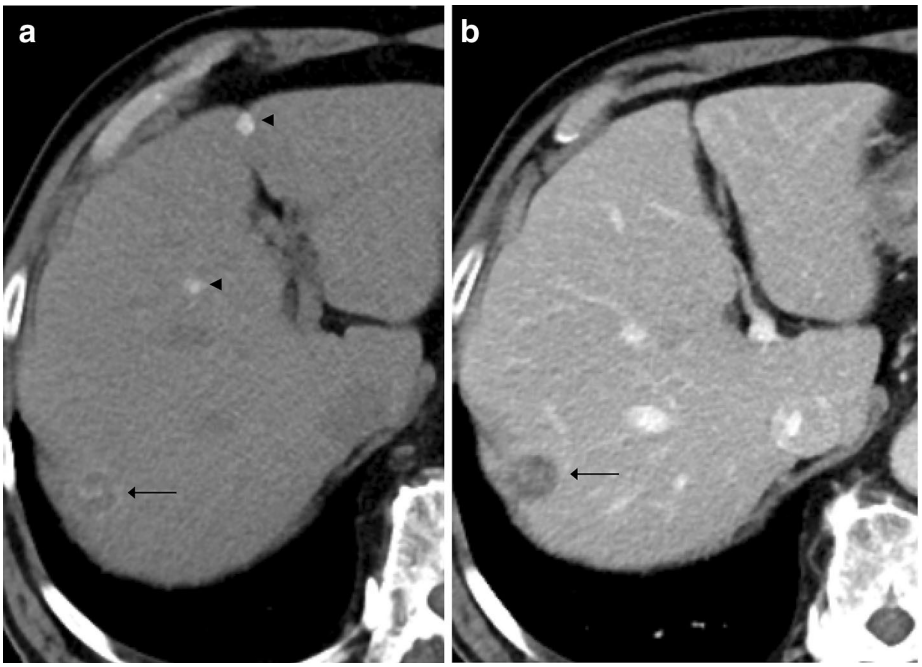

Fig. 2 **a**, **b** The second-largest hepatic nodule (black arrow) with a diameter of 15 mm in segment 7 presented similar radiological findings to the largest nodule in segment 3 previously mentioned in Fig. 1. Two other hyperattenuating nodules (arrow heads) were identified in segment 3 and 4, and had 7 mm and 5 mm diameters, respectively

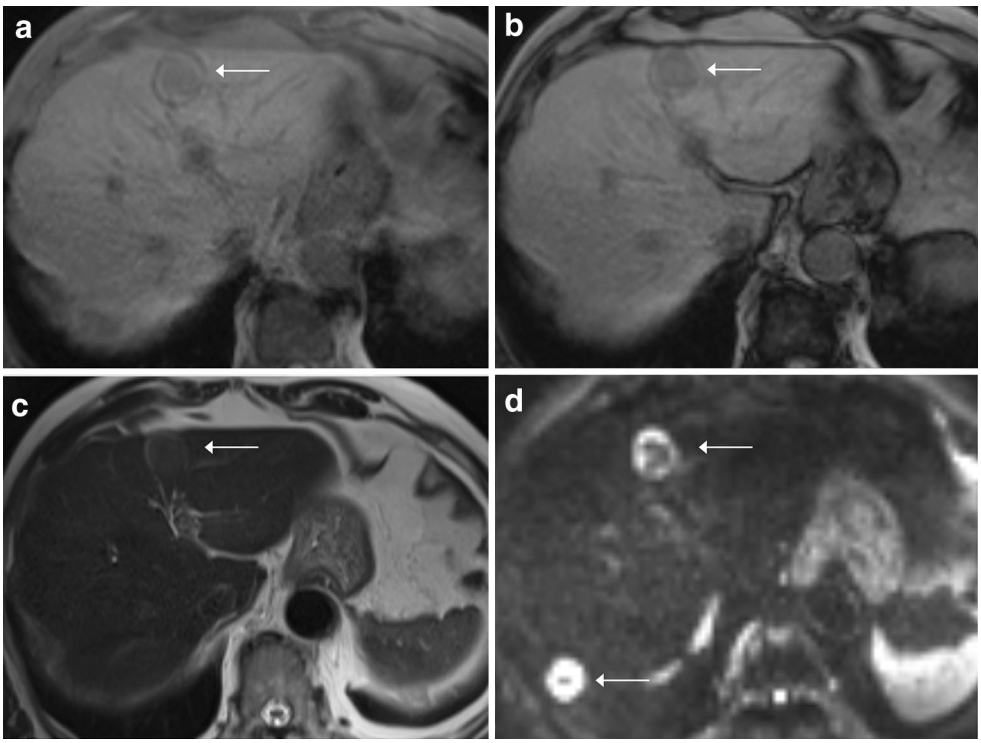

Fig. 3 Magnetic resonance imaging (MRI) of the upper abdomen. **a** On the in-phase of T1-weighted image, the largest nodule (white arrow) was hypointense relative to normal liver parenchyma with a peripheral hypo and hyperintense rim. **b** The opposed-phase of the T1-weighted image revealed that the nodule contained no lipid component. **c** T2-weighted image showed that the nodule in segment 3 was slightly hypointense to normal liver parenchyma with peripheral ring-like hyperintense area (**d**). Diffusion-weighted images showed the nodule had a peripheral rim-like hyperintense area. The second-largest nodule (black arrow) showed similar findings to the largest nodule

(TR/TE = 5855.7 ms/70 ms, ST = 5 mm, b value = 800 mm/s^2) showed the nodule had a central hypointense area with a peripheral rim-like hyperintense area (Fig. 3d). Gd-EOB-DTPA-enhanced image showed no enhancement in the arterial and portal phases, and obvious hypointensity with respect to normal liver parenchyma in the hepatobiliary phase (Fig. 4a–c). 18F-FDG PET/CT revealed no obvious increased uptake of nuclear species into the liver nodule (Fig. 4d). The second-largest nodule in segment 7 also had similar findings to the largest nodule in segment 3 on MRI and 18F-FDG PET/CT. The remaining two nodules were also hypointense on the T2- and T1-weighted MRI without contrast enhancement. 18F-FDG PET/CT also revealed a vivid accumulation area of nuclear species in the sigmoid

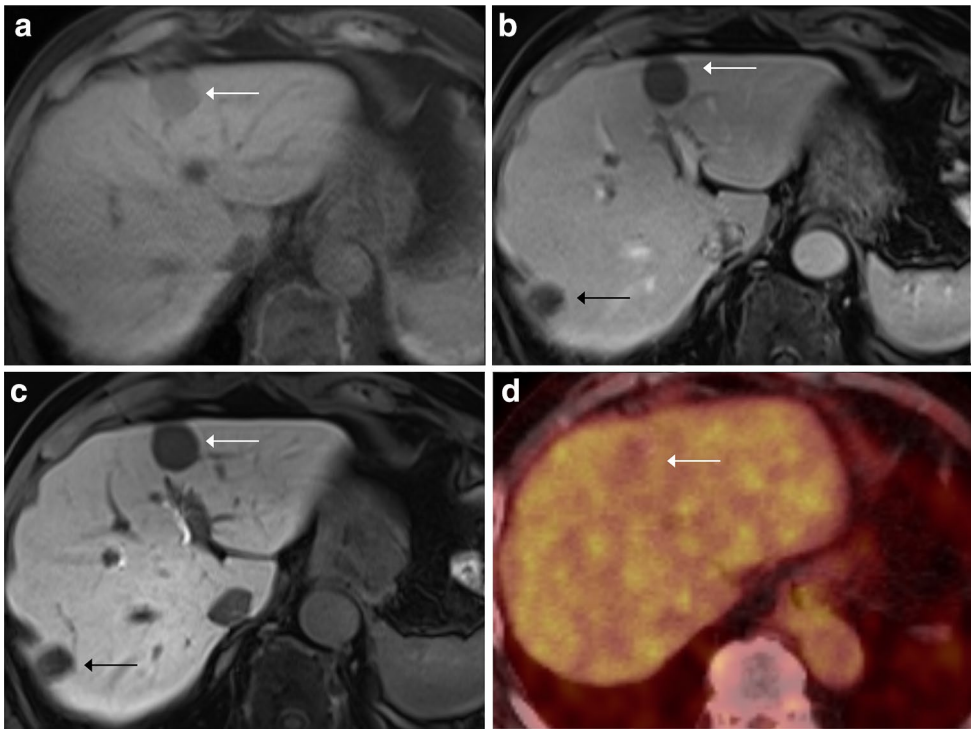

Fig. 4 Non-contrast (**a**) and gadolinium ethoxybenzyl diethylenetriamine pentaacetic acid enhanced images of MRI (**b**) showed no enhancement of the largest nodule in segment 3 in portal phase (white arrow). **c** The largest nodule (white arrow) revealed obvious hypointensity relative to normal liver parenchyma in the hepatobiliary phase. The second-largest nodule (black arrow) showed similar findings to the largest nodule (**b**, **c**). **d** 18-fluorine fluorodeoxyglucose positron emission tomography revealed no obvious increased uptake of nuclear species into the liver nodule (white arrow)

colon. Using a colonoscopy, we confirmed this lesion as an adenocarcinoma with a biopsy. No additional lesions were observed.

Although two largest hepatic nodules did not show findings typical of liver metastases from sigmoid colon cancer, it was difficult to exclude liver metastases because the hyperattenuating lesions of the nodules were similar to calcifications seen in metastatic adenocarcinoma of the colon. Therefore, we performed both a hepatic partial resection of the two largest hepatic nodules in segments 3 and 7 and a sigmoidectomy for the colon cancer. Although the remaining two hepatic nodules were suspected to be granulomas, the third largest, 7-mm nodule in segment 3 was resected because it was near the largest nodule.

On the resected specimen, all three resected nodules were yellowish-white round lesions. The representative nodule in segment 3 is shown in Fig. 5a. The nodules were mainly composed of central necrotic tissue with peripheral histiocytic aggregates (Fig. 5b). Calcium staining revealed widespread calcium deposition in the center of the nodules (Fig. 5c). Hematoxylin and eosin stain, mucicarmine stain (Fig. 5d), and periodic acid-Schiff (PAS) stain (Fig. 5e) showed numerous yeast-like cells, and therefore, we diagnosed the patient with cryptococcosis. A histologic capsule was not observed. The second- and third-largest nodules in segments 7 and 3 also had similar macroscopic and histological findings to the largest nodule in segment 3. Because fungal infection was not suspected before the surgery, we did not perform a culture of surgical specimens. Furthermore, malignant cells were not identified in the liver specimen. The cancer in the sigmoid colon had grown into the submucosa without lymphatic or vascular invasion. Lymph node or distant metastases were not evident. The final diagnosis of the colon cancer was stage I (T1, N0, M0) according to the TNM classification of the UICC 8th edition [11].

The patient did not undergo chemotherapy after the surgery nor did he receive antifungal treatment for cryptococcosis, because he did not have any symptoms. The smallest hyperattenuating nodule in segment 4 was not resected and remained unchanged, and hepatic cryptococcosis did not recur in any part of the body. The patient died from recurrence of the sigmoid colon cancer five years after the surgery.

Discussion

Cryptococcosis is a ubiquitous mycotic infectious disease caused by pathogenic encapsulated yeasts from the genus *Cryptococcus* [1]. Approximately 95% of cryptococcal infections in humans are caused by *Cryptococcus neoformans* [2]. This fungus affects both the immunocompromised and immunocompetent individuals. *C. neoformans* is distributed widely throughout the world and is association with excreta from birds such as pigeons [12] and soil amoeba [13] and in a variety of tree species. Infection usually occurs through inhalation of spores from environmental reservoirs with deposition into pulmonary alveoli. The

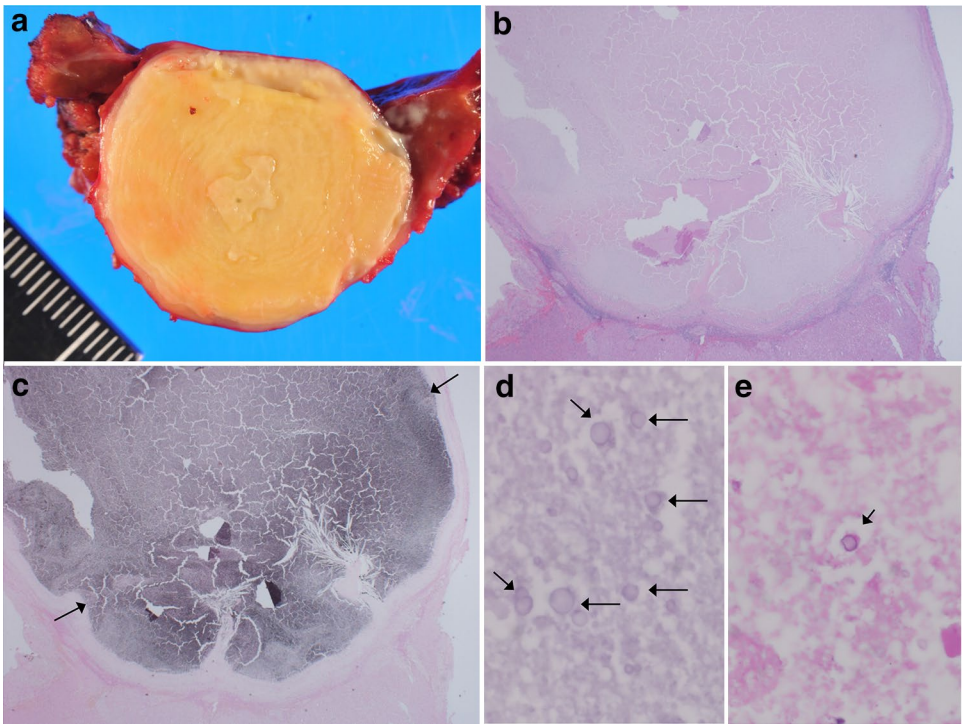

Fig. 5 Pathological findings. **a** On the resected specimen, yellowish-white round lesions were seen in segment 3 of the liver. **b** Hematoxylin and eosin (HE)-stained low-power field image showing that the nodule was mainly composed of central necrotic tissue with peripheral histiocytic aggregates. **c** Calcium-stained low-power field image showing widespread calcium deposition in the center of the nodule. **d**, **e** Mucicarmine (**d**) and periodic acid-Schiff (PAS) (**e**) stained high-power field images showed numerous yeast-like cells; thus, a diagnosis of cryptococcosis was made

yeast may potentially enter via the gastrointestinal tract. The most common sites of occurrence of this infection are the respiratory and central nervous system [2]. Cryptococcosis infrequently involves the skin, prostate gland, eyes, bones, and joints [2]. However, this yeast can widely disseminate in severely immunocompromised patients; therefore, it has the potential to involve any organ of the body.

Several cases of hepatic cryptococcosis have been reported as a manifestation of disseminated cryptococcosis in immunocompromised patients [7–10]. A few cases of hepatobiliary cryptococcosis manifesting as obstructive jaundice in an immunocompetent child have also been reported [14, 15]. Nara et al. [14] and Zhang et al. [15] reported hepatobiliary cryptococcosis manifested as an irregular, low-attenuated mass extending along the hepatoduodenal ligament with bilateral intrahepatic bile duct dilation, mimicking the cholangiocellular carcinoma or primary sclerosing cholangitis. However, to the best of our knowledge, cryptococcosis presenting as well-defined intrahepatic nodules without additional organ involvement has not been reported.

Although we are the first to report organized imaging findings of intrahepatic cryptococcosis, several cases regarding radiological findings of pulmonary cryptococcosis have previously been reported [3–5]. The most common CT findings of pulmonary cryptococcosis are pulmonary nodules [3]. These nodules are usually multiple and well-defined with smooth margins [4]. Cavitation of nodules is a frequent finding [4]. The nodules tend to be distributed peripherally [5] and lymphadenopathy is infrequent [4, 5]. In the present case, the hepatic nodules were well-defined with smooth margins and tended to be located in the peripheral region. Central necrosis was also observed. Similarities in radiological findings were observed between pulmonary and hepatic cryptococcosis. The hyperattenuating area observed on the CT image corresponded to the presence of calcium.

Hepatic involvement secondary to disseminated cryptococcosis occurs via a hematogenous infection pathway, while isolated hepatobiliary cryptococcosis may be a retrograde infection occurring via the biliary tract. In the present case, we could not identify a distinct infection pathway because the patient had no apparent history of contact with birds or their excreta.

In conclusion, we presented a unique case of isolated intrahepatic cryptococcosis in an immunocompetent adult. Radiologists should be aware that hepatic cryptococcosis may manifest as well-defined necrotic nodules with central hyperattenuation.

Author contributions All authors contributed to the study conception and design. The first draft of the manuscript was written by Sodai Hoshiai and all authors commented on previous versions of the manuscript. All authors read and approved the final manuscript.

Funding No funding was received for this study.

Compliance with ethical standards

Conflict of interest The authors declare that they have no conflicts of interest.

Ethical approval All procedures performed in studies involving human participants were in accordance with the ethical standards of the institutional and/or national research committee and with the 1964 Declaration of Helsinki and its later amendments or comparable ethical standards.

Informed consent Informed consent was obtained from the patient in the study.

References

1. Perfect JR, Dismukes WE, Dromer F, Goldman DL, Graybill JR, Hamill RJ, Harrison TS, Larsen RA, Lortholary O, Nguyen MH, Pappas PG, Powderly WG, Singh N, Sobel JD, Sorrell TC (2010) Clinical practice guidelines for the management of cryptococcal disease: 2010 update by the infectious diseases society of America. Clin Infect Dis 50(3):291-322. https://doi.org/10.1086/649858.
2. Maziarz EK, Perfect JR (2016) Cryptococcosis. Infect Dis Clin North Am 30(1):179-206. https://doi.org/10.1016/j.idc.2015.10.006.
3. Khoury MB, Godwin JD, Ravin CE, Gallis HA, Halvorsen RA, Putman CE (1984) Thoracic cryptococcosis: immunologic competence and radiologic appearance. AJR Am J Roentgenol 142(5):893-896.
4. Lindell RM, Hartman TE, Nadrous HF, Ryu JH (2005) Pulmonary cryptococcosis: CT findings in immunocompetent patients. Radiology 236(1):326-331. https://doi.org/10.1148/radiol.2361040460.
5. Xie LX, Chen YS, Liu SY, Shi YX (2015) Pulmonary cryptococcosis: comparison of CT findings in immunocompetent and immunocompromised patients. Acta Radiol 56(4):447-453. https://doi.org/10.1177/0284185114529105.
6. Lanzieri CF, Bangert BA, Tarr RW, Shah RS, Lewin JS, Gilkeson RC. (1997) Neuroradiology case of the day. CNS cryptococcal infection. AJR Am J Roentgenol 169(1):295299.
7. Rohtagi A, Aggarwal A, Chabra MK, Dahale AS (2013) Disseminated cryptococcosis with hepatic dysfunction as the initial manifestation in an immunocompetent adult. Arch Iran Med 16(5):303-305.
8. Lu S, Furth EE, Blumberg EA, Bing Z (2009) Hepatic involvement in a liver transplant recipient with disseminated cryptococcosis. Transpl Infect Dis 11(2):179-182. https://doi.org/10.1111/j.1399-3062.2009.00365.x.
9. Utili R, Tripodi MF, Ragone E, Casillo R, Pasquale G, De Santo L, Esposito S (2004) Hepatic cryptococcosis in a heart transplant recipient. Transpl Infect Dis 6(1):33-36.
10. Das CJ, Pangtey GS, Hari S, Hari P, Das AK (2006) Biliary cryptococcosis in a child: MR imaging findings. Pediatr Radiol 36(8):877-880.
11. Brierley J, Gospodarowicz M, Wittekind C (2016) TNM Classification of malignant tumours. 8th ed: Wiley-Blackwell.
12. Emmons C (1955) Saprophytic sources of Cryptococcus neoformans associated with the pigeon (Columba livia). Am J Hyg 62(3):227-232.
13. Steenbergen JN, Shuman HA, Casadevall A (2001) Cryptococcus neoformans interactions with amoebae suggest an explanation for its virulence and intracellular pathogenic strategy in macrophages Proc Natl Acad Sci USA 98:15245-15250.
14. Nara S, Sano T, Ojima H, Onaya H, Ikeda M, Morizane C, Esaki M, Sakamoto Y, Shimada K, Kosuge T (2008) Liver cryptococcosis manifesting as obstructive jaundice in a young immunocompetent man: report of a case. Surg Today 38(3):271-274. https://doi.org/10.1007/s00595-007-3605-6.
15. Zhang C, Du L, Cai W, Wu Y, Lv F (2014) Isolated hepatobiliary cryptococcosis manifesting as obstructive jaundice in an immunocompetent child: case report and review of the literature. Eur J Pediatr 173(12):1569-1572. https://doi.org/10.1007/s00431-013-2132-2.